PCCP

Accepted Manuscript

ROYAL SOCIETY OF CHEMISTRY

www.rsc.org/pccp

PCCP

RSCPublishing

PERSPECTIVE

In situ Raman and Surface-enhanced Raman spectroscopy on working electrodes: spectroelectrochemical characterization of water oxidation electrocatalysts

Cite this: DOI: 10.1039/x0xx00000x

Received ooth January 2012,
Accepted ooth January 2012

DOI: 10.1039/x0xx00000x

www.rsc.org/

Khurram S. Joya,*[a,b] Xavier Sala[c]

In situ Raman and surface-enhanced Raman scattering (SERS) are established vibrational spectroscopic techniques with wide application in the field of chemical, material and life sciences. Their particular characteristics make them especially useful when dealing with catalytic water oxidation at anodes. The in situ characterization of the fate of electrocatalysts (whether molecular or oxide materials) employed under reaction conditions is crucial to determine the chemical identity and physical state of the actual catalytic species. Such studies also help on both, attaining mechanistic insights underlying the catalytic reaction and confirming/discarding the possibility of molecular to colloidal or heterogeneous phase conversions taking place prior or under turnover conditions. This perspective article highlights the use of in situ Raman and SERS as principal spectroscopic tools in the electrocatalysis field by means of recent contributions where they are employed to in operando characterize both molecular and oxide-based water oxidation electrocatalysts. These in situ spectroscopic measurements support in assessing both the progressive oxidation and the structural evolution of the employed catalytic species under electrochemical conditions. Therefore, this article provides an informative guideline for developing in situ spectroelectrochemical methods to study and characterize water oxidation catalysis at working anodes.

1. Introduction

Recently, there is a lot of ongoing research in the field of artificial photosynthesis to develop a solar to fuel conversion system. One key component still considered the bottleneck of such a device is a bioinspired water oxidation catalyst (WOC).[1,2] Despite the thermodynamically and kinetically demanding character of the reaction, significant catalysts have appeared over the last five years both based on molecular systems[3,4] and on oxide materials.[5-7] When molecular redox catalysts are employed the catalytic species are immersed in a continuous cycling among several oxidation states that, together with the harsh conditions required to drive these oxidations, often lead to the instability of the catalytic system. This can certainly result in catalyst degradation but can also be the source of new and sometimes superior catalytic species formed in situ. In fact, in situ generated molecular complexes and metal-oxide catalysts have been repeatedly reported as highly active water oxidation catalysts.[8,9] Therefore, the precise understanding of the

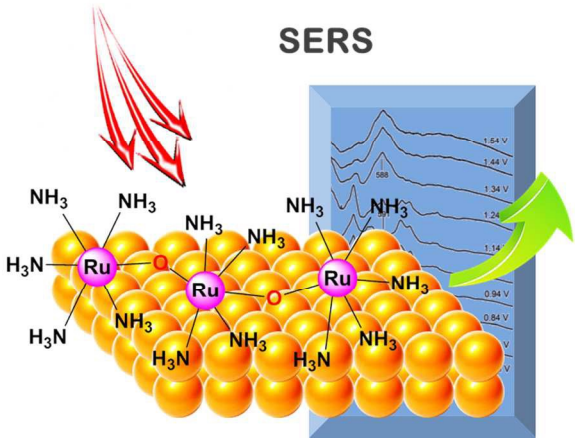

Fig. 1 Surface-enhanced Raman spectroscopy (SERS) for a molecular trinuclear Ru-based water oxidation complex on an Au substrate.

changes experienced by a molecular WOC while oxidatively activated and under turnover conditions is key in order to

identify the nature (single or multiple-site) and the structure of the real active species and its reaction mechanism, thus allowing ulterior rational catalyst improvement. However, this is an arduous task requiring precise control of the reaction conditions and a combination of characterization techniques applied in operando and in a systematic manner.[10]

Cerium(IV) in the form of cerium ammonium nitrate (CAN) is still the most commonly used sacrificial reagent or primary chemical oxidant for the catalytic evaluation of WOCs. During the four-electron oxidation of water, an adequate amount of CAN is required to oxidatively activate the catalysis. However, it is also known that excess Ce(IV) in aqueous catalytic solutions can promote the formation of oxo- and/or hydroxo-bridgded dinuclear complexes form the initial mononuclear species, thus complicating the catalytic cycle and the attainment of molecular insight of the reaction mechanism. Furthermore, the use of this oxidant in water oxidation studies has several other drawbacks such as; (1) its huge standard redox potential (1.72 V vs SHE) that can easily oxidize the organic ligands of molecular complexes and therefore decompose/transform the whole catalyst architecture,[11,1,2] (2) the capacity of its nitrate anions to contribute as a source of oxygen under certain conditions,[13] and (3) the variation of the applied oxidizing power along the reaction coordinate due to the changing relative concentrations of the Ce(IV) and Ce(III) ions present in solution.[14] These factors difficult the already challenging task of determining the nature, structure and reaction mechanism of the studied WOCs.

On the other hand, a totally different situation arise when using electrochemically-driven WOCs. In this scenario, the catalytic species are anchored or adsorbed onto electrode surfaces, as is for instance the case in surface-immobilzed molecular systems or when inorganic oxides are deposited onto electrode surfaces.[9-12] The electrochemical triggering of WOCs avoids the use of indiscriminate chemical oxidants an the applied potentials (and overpotentials) can be thoroughly controlled on demand. Therefore, with a controlled-increment of the applied potential under electrochemical conditions the progressive oxidation and structural evolution of molecular and inorganic heterogeneous WOCs can be monitored.[2] However, the in situ characterization of the species formed at an electrode surface under a certain applied potential is not straightforward, requiring specific in operando spectroscopic techniques of adequate sensitivity.

The electrochemical route of studying water oxidation catalysis can be further supported using in situ spectroscopic measurements for assessing the oxidative transformations and to probe the active molecular species or heterogeneous phase and their potential induced oxidations under catalytic turnover condition.[13,14] In this respect, in situ Raman and particularly surface-enhanced Raman scattering (SERS) have been gaining relevance as useful spectroscopic tools in the field of water oxidation catalysis.[14-17] SERS is particularly suitable for (and limited to) the study of water oxidation anodes where the catalyst is placed close to a signal-enhancing substrate (see Fig. 1 and Section 2 for further details). As a form of Raman spectroscopy benefits from high molecular specificity and, contrary to IR, from the non-interference of water and a high sensitivity in the low frequency range (where M-OH, M-OH_2 and M=O vibrations appear). Therefore, the SERS analysis of water oxidation anodes (both bearing molecular or oxide catalysts) provides a wealth of in operando structural information highly valuable to figure out the identity of the real active catalysts (including the monitoring of potential molecular to heterogeneous phase conversions before or during O-O bond formation) and even their reaction pathways. Therefore, this perspective is intended to highlight the potential of in situ Raman and SERS in the field of water oxidation catalysis by means of noteworthy and interesting examples of their applications. As excellent recent reviews focused on the SERS phenomenon exist,[18] only a brief and qualitative description of the technique is given in Section 2. Four ilustrative recent studies follow in Section 3 where in situ Raman and SERS are used to in operando characterize both molecular (the trinuclear ruthenium complex Ru-red and a single-site molecular Cp*-Ir^{III} catalyst) and oxide-based (Co-oxide and Ni-Fe oxide) water oxidation electrocatalysts.

2. Raman spectroscopy and surface-enhanced Raman scattering (SERS)

Raman spectroscopy is a vibrational spectroscopic technique that observes vibrational, rotational, and other low-frequency modes.[18] After its discovery almost 85 years back, Raman spectroscopy has become a major vibrational spectroscopic technique and has acquired many applications in the field of chemical sciences.[19] The principle of Raman spectroscopy relies on the inelastic (or Raman) scattering of single wavelength light while ineracting with a material. Monochromatic light from a laser source (usually in the visible, near infrared, or near ultraviolet range) interacts with the molecular vibrations, phonons or other excitations in the material, causing up or down shifts in the energy of the incident laser photons. These energy changes provide very useful information about the vibrational modes present in a given system.[18,20] Thus, Raman spectroscopy is a valuable tool in chemistry and materials science owing to its capacity to help on the identification of molecular species by means of their spectroscopic fingerprint. Commonly used energy range for Raman scattering is from 200 - 4000 cm^{-1}.

With time, many advanced forms of Raman spectroscopy have been developed not only to enhance the sensitivity and the spatial resolution of the technique but also to acquire specific information. These variations include surface-enhanced Raman spectroscopy, resonance Raman spectroscopy, tip-enhanced Raman, stimulated Raman, transmission Raman, spatially offset Raman, and hyper Raman.[20,21]

During the last few decades, surface-enhanced Raman spectroscopy has become a recognised and mature vibrational spectroscopic technique, especially in chemical and life sciences and in materials characterization.[18] Surface-enhanced Raman scattering or surface-enhanced Raman spectroscopy is a surface-sensitive technique that enhances the Raman scattering of molecular species adsorbed or brought into close proximity to coarse or rough metal surfaces such as Pt, Au or silver.[22] The SERS phenomenon was first observed in 1974 at the University of Southampton (Southampton, UK) while working on submonolayers of small nonresonant organic molecules, such as pyridine, adsorbed on electrochemically roughened silver surfaces.[23] In fact, the mandatory presence of metal nanostructures is the most prominent difference between normal and surface-enhanced Raman spectroscopies. However, this technical requirement can be exploited in fields such as spectroelectrochemistry and electrocatalysis, among others. Therefore, for instance, an electrochemically roughened polycrystalline gold or silver substrate may act as both, an appropriate surface to be used as working electrode and a Raman scattering enhancement factor (which can be as high as 10^{10} to 10^{11} times that of the unenhanced signal). The huge enhancement of the inelastic scattering processes allows detecting even single molecules by SERS analysis.[23,24]

Mechanistic and experimental considerations of surface-enhanced Raman scattering

SERS is a powerful and non-destructive spectroscopic technique that provides chemical and structural information when few or even single molecular species are placed at the appropriate surfaces.[15,19] The precise mechanistic theory behind signal enhancement in SERS is still debatable. However, two primary contributions (electromagnetic and chemical) are currently generally accepted. but their mechanisms vary significantly, and it is a challenging task to distinguish them by experimental methods.[18] Briefly, the electromagnetic contribution of signal enhancement is based on the pure physical interaction of light and nanostructured mater, which end up generating huge local electic fields through the excitation of localized surface plasmon resonances (LSPRs). These electric fields then emit amplified light that is inelastically scatterd by molecules generating the SER spectra. The electromagnetic effect is by far the most dominant contribution, with signal enahancements from 3 to 10 orders of magnitude. In short, this effect can be described as a signal enhancement due to plasmon-assisted scattering of molecules.[18] On the other hand, the chemical contribution is a minor signal enahancement factor (form 1 to 3 orders of magnitude) based on the effect of the direct contact of molecules and nanostructured metal surfaces and, particularly, on the increase of the electronic polarizability of the adsorbed molecule due to; (a) charge-transfer from the molecule in its ground state to the metal surface and, (b) a change in the energy levels of the adsorbed molecule from the "unbound" to the "bound" situation.[18] For further details about the chemical and electromagnetic enhancement factors in SERS see Ref. 18 and references therein.

In order to properly generate the enhanced Raman signal the experimental setup of a SERS study requires simple but careful consideration of both the sample to be analyzed and the employed optical apparatus. guaranteeing optimal generation of SERS signal and their enhancement.[19] About the latter, one of the foremost parameters to take into account is the selection of an appropriate signal enhancing material (also named the SERS substrate). As general characteristics, SERS substrates must be chemically stable, easy to prepare in a reproducible manner and able to generate high and uniform local electric fields upon irradiation. They are selected acquired to posses tunable plasmon resonances and a whole spectrum of average SERS enhancement factors. Coarse or rough metal surfaces based on Pt, Au and Ag generally fulfil these requirements and are specially suitable due to their stability and inertness under diverse chemical environments. Cu is also employed but its high chemical reactivity limits its applications. As shown in Fig. 2, copper, gold and silver have LSPRs that encompass most of the wavelength range (visible and near infrared) where most Raman measurements take place. This fact convert these metals in attractive SERS substrates.

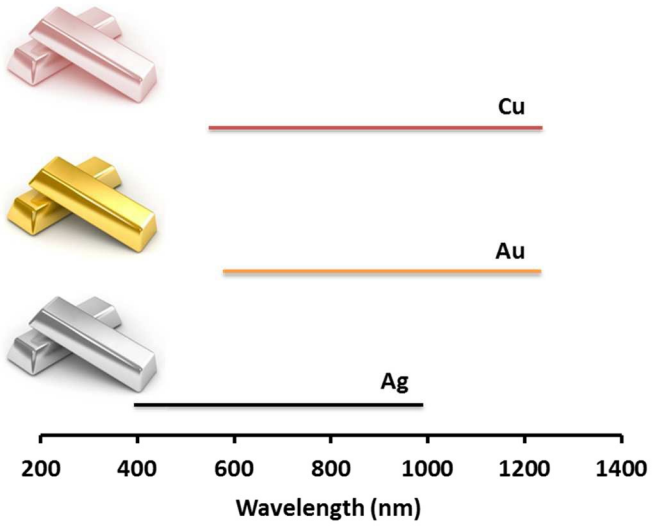

Fig. 2 Estimated wavelength ranges where Cu, Au and Ag substrates have been well-characterized and are established to support SERS measurements. (adapted from Ref. 19)

Structurally, SERS substrates may range from nanoparticle and nanorods to three-dimensional colloidal phases with tunable LSPRs and diverse enhancement factors.[18,19] It is worth to mention that the maximum signal enhancing region is reduced to few nanometres from the substrate surface, fastly decreasing with distance. This clearly determines the placement of the sample within the experimental set up and explains why the results of SERS characterization are highly dependent on how the adsorbed molecules interact with the plasmonic nanostructured surfaces.[25] Substrates such as gold and silver can be roughened by electrochemical methods during repetitive

oxidation−reduction cycles in 0.1 M potassium chloride (KCl) solution.[26] In the case of a polycrystalline gold substrate this method yields a brownish textured surface that provides particularly high signal enhancements.. Furthermore, molecular sample on a particular surface should prepare in a way to have a close proximity to the SERS substrate, as the best SERS enhancement effects are originated in a configuration where molecules are positioned few nanometers away from the surface or the SERS substrate.[27,28]

Next to the substrate, the choice of a suitable excitation source or laser light to efficiently excite the LSPRs is also key for maximizing signal enhancement. While theories predict that a maximum SERS enhancement effect occurs when the laser is tuned to the highest point of the plasmon resonance. Experimental data show that maximum enhancement factors are found when the laser wavelength is shifted to the blue of the plasmon resonance, preferably shifted by one-half of the original Raman vibrational frequency.[27] This efficiently maximize both the excitation and emission parts of the Raman process. Thus, a red-shift tuning of the plasmon frequency from the laser wavelength cause maximum Raman signal enhancement. Finally, the detection of the enhanced scattered light is another important part of the SERS setup. Here the process is identical to that on normal Raman experiments where Rayleigh scattering is captured/reflected by long-pass filters and the transmited Raman signal is then detected. The signals are ultimately processed by a spectrograph and a detector facilitate the imaging process of the Raman spectra across a wide spectral region.[**Error! Bookmark not defined.**]

3. Spectroelectrochemical characterization of water oxidation electrocatalysts by in situ Raman and surface-enhanced Raman studies

As stated in Section 1, the oxidation of water is the key half-reaction when the sustainable production of hydrogen from water and sunlight is envisaged. Therefore, strong efforts are nowadays devoted to the development of catalysts capable of efficiently carry out this reaction, which have to handle multiple electrons and protons and at the same time manage to make O-O bonds. Despite important progress have been made in the last five to ten years employing both molecular[**Error! Bookmark not defined.**] and oxide-based pecies,[28] catalyst combining fast cycling, long stability and low overpotentials are still scarce. However, it is obvious that the rational development of such a superb catalysts depends on the thorough understanding of the fate, physical nature and reaction mechanisms of the ones now available.[29] In this respect, in situ spectroelectrochemical methods such as in situ Raman and SERS measured during potential sweeping are helpful characterization tools to attain this information for electrochemically-driven catalysts (water oxidation anodes), both prior and under turnover conditions.[14-17] Therefore, we highlight in this section four ilustrative recent studies where these in situ techniques play a key role on the analysis of both molecular and oxide-based water oxidation electrocatalysts.

Characterization of heterogeneous thin-film Co-oxide electrocatalysts by in situ Raman spectroscopy

Cobalt oxides and their derivatives mixed/doped with other transition metals exhibit very good electrocatalytic activity in water oxidation.[30] However, increasing the catalytic efficiency by reducing their usually high overpotentials is still a current challenge.[31] In this respect, the group of A. T. Bell in Berkeley undertook detailed mechanistic studies conceived to identify the elementary processes contributing to water oxidation overpotentials and their relationship with the composition and morphology of the used anode.[15,16] In these contributions the acquisition of SER spectra during positive potential sweeping allows getting insight about the real active species and the particular oxidations and phase transitions taking place at different applied potentials. Therefore, as first selected example of this section we comment on the report of Yeo et al, focused on how metals can be used to enhance the electrocatalytic water oxidation activity of metal oxides.[15] Previous reports had considered the attainment of Co(IV) as a potential requirement for oxidizing water with Co oxides.[32,33] Therefore, the combination of CoO_x with highly electropositive metals such as Au could help on attaining this oxidation state. Furthermore, being Au a well known SERS substrate, the preparation of CoO_x deposited on Au electrodes allows the authors to spectroelectrochemically characterize the composition and evolution of the CoO_x species prior and under turnover conditions by applying progressive potential increments. As can be observed in Fig. 3, bare Co and Au surfaces together with Au on which ~0.4 and ~87 monolayers (ML) of CoO_x were deposited are analysed by in situ Raman spectroscopy at different applied potentials.[15]

In 0.1M KOH at 0 V the in situ Raman spectrum of a bare Co surface (Fig. 3a) shows peaks at 197, 485, 620, and 691 **cm^{-1}**, which are assigned to the vibrational modes F_2g, Eg, F_2g, and A_1g, respectively, of spinel-type Co_3O_4. Furthermore, the sharp peak observed at 505 cm^{-1} is attributed to CoO(OH) thanks to previous Raman data[34,35] and the electrochemical observation of this oxide on the surface of Co_3O_4.[36] Increasing the applied potential to 0.7 V (where oxygen evolution occurs) implies the gradual depletion of Co_3O_4 (as evidenced by the disappearence of its Raman bands) and the formation of two new peaks at 503 and 565 cm^{-1}, ascribed to the formation of a CoO(OH) phase.[32,34] At higher anodic potential >0.8 V (not shown), the Raman spectrum is very similar to that observed at 0.7 V (Fig. 3a), exhibiting a sharp peak at 503 cm^{-1}. This data allows concluding that under oxygen evolution conditions; (1) the cobalt surface is predominantly covered by CoO(OH), and (2) there is no evidence for the formation of a well-defined Co(IV) oxide phase, which is in strike contrast to the results previously reported before based on in situ Mössbauer spectroscopy showing the coexistence of Co(III) and Co(IV) phases during the oxygen evolution reaction (η = 318 mV).[37] On the other

hand, when a bare Au substrate is analysed through in situ Raman spectroscopy gold oxide formation is only observed at potentials above 0.2 V (Fig. 3b).

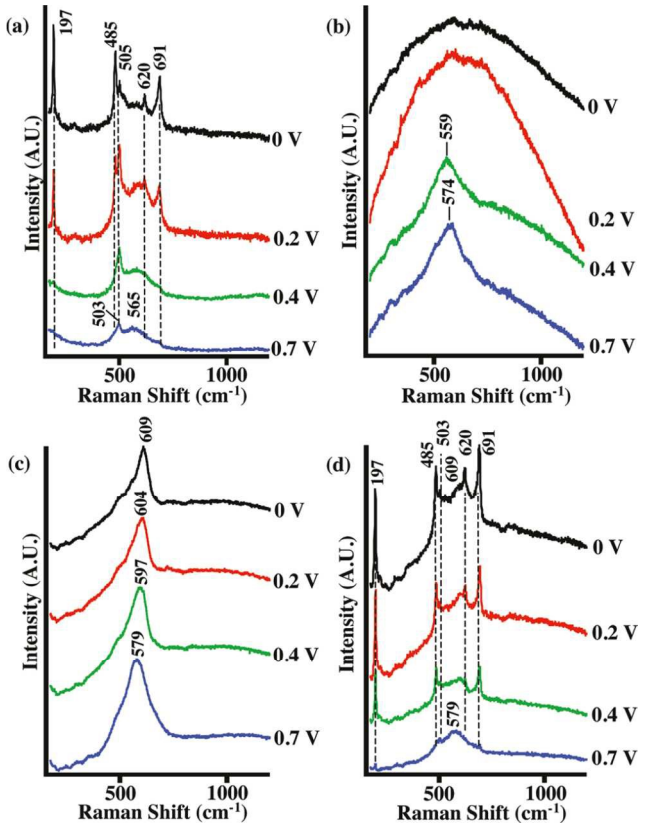

Fig. 3 Potential-dependent in situ Raman spectra in 0.1 M KOH for (a) bare Co, (b) simple Au substrate, (c) ~0.4 ML cobalt oxide deposited on Au, and (d) ~87 ML cobalt oxide deposited on Au. Raman spectra were collected during linear sweep voltammetry at a scan rate of 2 mV s^{-1}. (with permission from ACS)

When ~0.4 monolayers of cobalt oxide are deposited on an Au substrate a sharp Raman band at 609 cm^{-1} is observed at 0 V (Fig. 3c). This peak monotonically red-shifts to 579 cm^{-1} as the potential is increased to 0.7 V, which indicates the synchronous oxidation of the surface species.[15] The assignment of this Raman feature (609-579 cm^{-1}) to CoO_x species that progressively increase their oxidation state from the inicial Co(II) and/or Co(III) until Co(IV) due to the applied redox potential is based on similar Raman red-shifts reporded for: (1) the oxidation of $LiCoO_2$ to Co(IV), and (2) the oxidation of CoO_x in a O_2/Ar plasma when the mole fraction of O_2 increase. On the other hand, when the cobalt oxide content on the Au substrate is increased to ~87 monolayers, the Raman features observed (Fig. 3d) are a mix of those observed for bare Co (Fig. 3a) and for ~0.4 monolayers of cobalt oxide on Au. Thus, Co_3O_4 dominates at 0 V and is electrochemically converted into CoO(OH) when rising the redox potential (band at 503 cm^{-1}). However, the intense Raman band observed at 579 cm^{-1} is assigned, as explained above, to CoO_x (Co(IV)) type of species.[15,38] Thus, it is concluded that the electro-deposited cobalt oxide layer exhibits a Co_3O_4 phase, which is oxidized to a CoO(OH) type of phase and finally to Co(IV) with increasing anodic potential.

Correlation of the in situ spectroelectrochemical analysis of the prepared anodes with the results of their capacity as water oxidation electrocatalysts allowed the authors conclude that the close contact of cobalt oxides with Au surfaces (~0.4 ML case) assist their electrochemical oxidation and increase the surface Co(IV) population, being this oxidation state key for the observed enhancement of the electrocatalytic activity (TOF increase nearly 40 times with regards to bulk Co).[15]

In situ Raman characterization of Ni and Ni-Fe oxides as electrocatalytic materials

Nickel oxide derived anodic materials are among the most active electrocatalysts for oxygen evolution in near-neutral and alkaline conditions.[39,6] Like is the case for cobalt oxide WOCs, nickel oxide anodes undergo progressive oxidation as function of the applied redox potential.[16,30] Therefore, in order to rationally improve the existing catalytic systems based on this earth abundant element it is crutial to figure out the structure of the active oxide phases. Of special interest are mixed Ni-Fe oxides, which have been reported to markedly reduce the needed overpotentials for water oxidation.[40] However, little was known about their structure under oxidative/turnover conditions. Taking all this into account and following their work on cobal oxides discussed above, Bell and co-wokers decided to shed some light on the structure-activity relationships of these interesting catalysts by combining electrochemical and spectroelectrochemical (SERS) characterization tecniques with electrochemically-driven water oxidation experiments.[16]

Prior to the in situ Raman characterization of Ni-Fe catalysts, a thorough SERS analysis of the spectral changes occurring on simpler Ni and Fe films during positive potential sweeping was initially carried out. In 0.1M KOH and at 0 V the in situ Raman spectrum of a Ni film shows bands at 449, 494 and ~530 cm^{-1} (Fig. 4a, Ni-O vibrations) and in the 3581-3668 cm^{-1} region (Fig. 4b, O-H vibrations) that are consistent (both in energy and shape) with a disordered pre-catalyst based on α-$Ni(OH)_2$ or a disordered form of β-$Ni(OH)_2$.[16,41-42] At about 0.47 V (vs. Hg/HgO) this species transforms into NiOOH, with intense Ni-O vibrations appearing at 474 and 554 cm^{-1} that could in principle belong to both γ-NiOOH and β-NiOOH phases.[16,41] The correspondence of these two bands to the presence of a γ-NiOOH phase at high potentials is proposed by the authors due to: (1) their relative intensities (I_{474}/I_{554} is reported to be higher in the γ-phase),[16,43] and (2) the measured Ni oxidation state of 3.2 for as-deposited Ni layers. Contrary to the Ni case, little information was extracted from the quite static and broad SER spectra at different applied potentials of a thin Fe film (not shown).

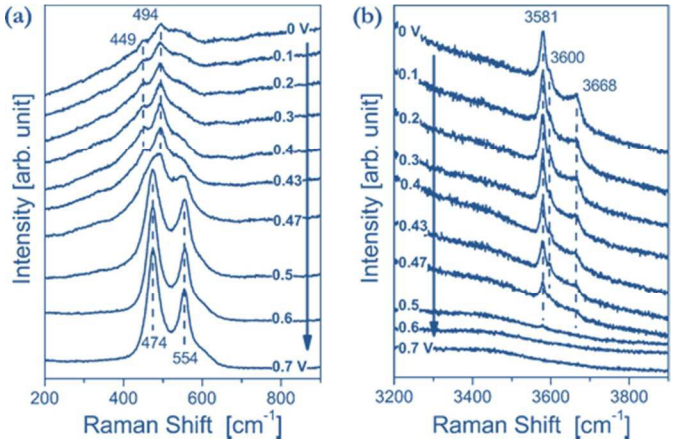

Fig. 4 Potential-dependent in situ Raman spectra measured at (a) low wavenumber and (b) high wavenumber regimes of Ni thin films on a roughened gold substrate in 0.1 M KOH. (the onset potential for oxygen evolution is 0.365 V vs. Hg/HgO). (with permission from ACS)

Ni-Fe mixed metal oxides of different compositions where then analysed electrochemically (CV) and spectroelectrochemically (SERS) in basic electrolytes. As shown in Fig. 5 in situ Raman spectra of the bimetallic catalysts were aquired at two different potentials, 0.2 and 0.6 V vs. Hg/HgO, potentials located at both sides of the observed $Ni(OH)_2/NiOOH$ couple, prior (0.2 V) and under (0.6 V) turnover conditons. that corresponds to oxygen evolution reaction (η = 235 mV) are collected in alkaline condition (Fig. 5). At low potential (0.2 V) the evolution of the Raman spectra with regards to the Ni/Fe ratio at both low (Fig. 5a) and high (Fig. 5b) wavenumbers allows concluding that: (1) no new phases containing both Ni and Fe are formed (the Raman features observed can be assigned to those previously observed for each metal), and (2) the increase on the Fe content provokes a progressive disordering of the $Ni(OH)_2$ species (conversion of the sharp Raman bands corresponding to β-$Ni(OH)_2$ at 450, 494 and 3580 cm^{-1} to more broad bands assigned to less ordered $Ni(OH)_2$ phases).[16]

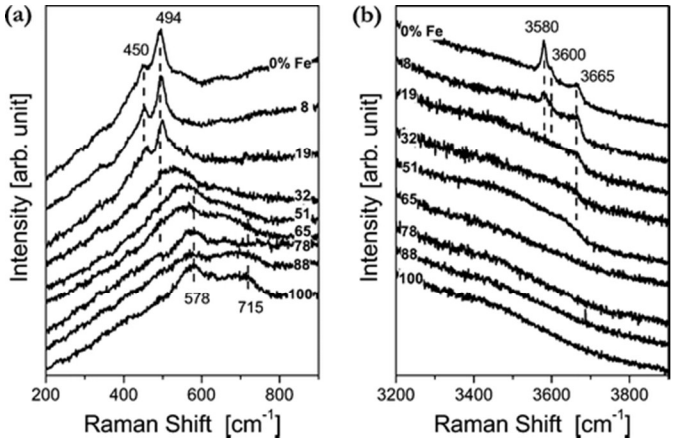

Fig. 5 Compositional-dependent in situ Raman spectra measured in 0.1 M KOH at (a) low and (b) high wavenumber regions for Ni−Fe catalysts at a potential of 0.2 V vs Hg/HgO (1 M KOH). (with permission from ACS)

On the ther hand, observing the evolution of the Raman spectra with regards to the Ni/Fe ratio under turnover conditions (0.6 V vs. Hg/HgO, Fig. 6a) together with the aging effect on the Raman bands for a Ni film at the same potential (Fig. 6b), allows extracting the following interesting information: (1) NiOOH is present under turnover conditions but its structure is modified by the progressive introduction of Fe (merging of the two characteristic bands at 475 and 555 cm^{-1} together with a decrease in their I_{475}/I_{555} ratio and the appearance of a new band at 494 cm^{-1}), (2) aging of a Ni film has the same effect than introducing Fe to this metal (decrease in the NiOOH I_{475}/I_{555} band ratio) and (3) formation of $NiFe_2O_4$ (previously suggested as potential active species in Ni-Fe WOCs) is not observed as no bands at 490 and 700 cm^{-1} are present at this potential.[44]

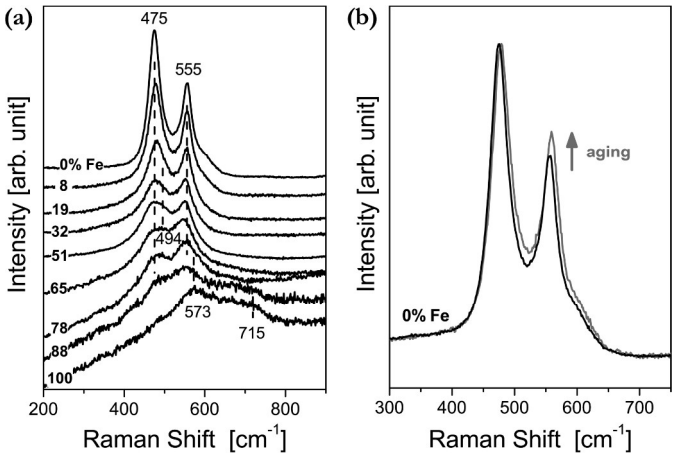

Fig. 6 In situ Raman spectra collected in 0.1 M KOH at an oxygen evolution overpotential of 0.235 V, or 0.6 V vs Hg/HgO (1 M KOH) for (a) Ni−Fe films of different composition and (b) an aged Ni film [shown in comparison to the as-deposited Ni film from (a)]. (with permission from ACS)

Finally, the authors correlated all the previous in situ Raman data with electrocatalytic water oxidation measurements employing the set of Ni-Fe anodes of different composition. This allowed stablishing key structure-activity relationships for this family of mixed oxides that can be summarized in the following points: (1) Ni-Fe oxide electrocatalysts have NiOOH as active species. (2) Fe modifies the structure of the latter species generating somehow disordered (or amorphous) β-NiOOH phases with enhanced water oxidation activity (up to 2 orders of magnitude with respect to monometallic Ni-oxides). (3) Ni-O vibrations (particularly the intensity ratio bethween the bands at 475 and 555 cm^{-1}) can be used in Ni-Fe systems as indicators of water oxidation activity (the lower the ratio the better the activity). Consequently, water oxidation pathways involving oxygen adsorbed intermediates at the Ni site are proposed.

SERS studies for the trinuclear Ru-Red catalyst

In 2013 we pioneered in characterizing a di-μ-oxo-bridged trinuclear ruthenium complex, $[(NH_3)_5Ru^{III}–O–Ru^{IV}(NH_3)_4–$

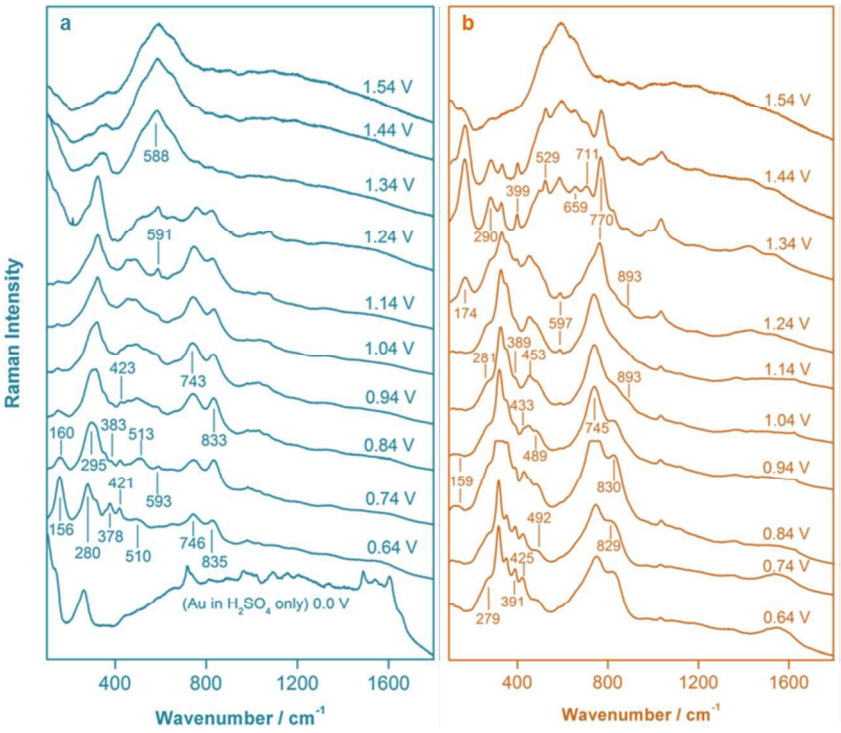

Fig. 7 Potential-dependent SERS data for (**a**) a roughened Au_{disk} in 0.1M H_2SO_4 solution containing 0.035 mM Ru-red and, (**b**) a Ru-red functionalized Au_{disk} in deoxygenated and Ar-saturated 0.1M H_2SO_4 solution (without Ru-red).

$O–Ru^{III}(NH_3)_5]^{6+}$, also known as Ru-red (Ru^{III}-O-Ru^{IV}-O-Ru^{III}), during electrocatalytic water oxidation using in situ SERS on an electrochemically roughened gold surface.[17] Ru-red is among the earliest molecular catalysts studied for water oxidation. It was described that this Ru complex undergoes, in aqueous acids, electro-induced oxidative conversion into a higher oxidation state compound, Ru-brown (Ru^{IV}-O-Ru^{III}-O-Ru^{IV}), before catalytically oxidizing water to dioxygen. However, the structural changes suffered by Ru-red during this transition were fairly unclear with the available data.[17,45] Figs. 7a and 7b show the SER spectra of solution phase Ru-red (0.1M H_2SO_4) on roughened gold and of a Ru-red functionalized Au electrode (RRA) without Ru-red in solution, respectively, at selected applied potentials. Below 0.70 V, the bands at 156 cm^{-1} (assigned to the Ru–O stretching mode) and at 280 cm^{-1} (O–Ru–N bending vibration) are characteristic of the presence of Ru-red. The dominance of the 156 cm^{-1} band at low potentials is indicative of the presence of Ru-red in close proximity to the gold electrode. Smaller features at 378, 421 and 510 cm^{-1} could correspond to Raman peaks for either Ru-red or Ru-brown, but signals at 746 and 835 cm^{-1} are characteristic for Ru-red (Fig. 7a). Therefore, considering the observed dominance of the modes at 156, 280, and 746 cm^{-1}, the species most prominently observed nearby the Au_{disk} in the low potential regime is Ru-red.[17]

As the potential is stepped up, the Ru–O stretching vibration shifts from 156 to ~175 cm^{-1} (Fig. 7b), peak previously observed for Ru-brown at 177 cm^{-1}[46] and initially absent at 0.64 V (Figs. 7a, 7b). Similarly, the Raman band at 280 cm^{-1} (at 0.64 V) also shifts to higher wavenumbers (294 cm^{-1}) at higher electrode potential, which infers the presence of Ru-brown at potentials greater than ca. 0.70 V vs. NHE (Fig. 7b). Compared to the SER spectra on the Au_{disk} with Ru-red in solution (Fig. 7a), the SERS analysis of RRA (without Ru-red in the electrolyte solution) reveals a delayed formation of Ru-brown (Fig. 7b) and suggests the different evolution of Ru-red in the two systems studied. Therefore, when Ru-red is only adsorbed on the Au surface and not present in solution the Ru-red/Ru-brown transition occurs at significantly more positive potentials. This delay in the oxidation behaviour is mirrored by the catalytic activity, which also starts at higher potentials for the RRA case.[17] Furthermore, the latter system shows Raman active modes which resemble the Raman features detected for ruthenium oxide during electrochemical oxidation.[47] Such RuO_x Raman modes are not observed in the SER spectra of Ru-red in solution.[17] Finally, when potentials over 1.34 V are applied to the RRA system, additional Raman peaks are observed at ca. 529, 659 and 711 cm^{-1}. These modes may be assigned to the generation of decomposition products or other monomeric species in the catalyst layer.[46]

Electrochemical SERS investigation for an Iridium-N-dimethylimidazolin-2-ylidene WOC

Organometallic Cp*-Ir^{III} derived WOCs have been matter of debate, especially their potential decomposition to IrO_x nanoparticles or metal oxides, the nuclearity of the active species when molecular in nature, and the oxidative stability of their Cp* ring under catalytic conditions.[11,48-49] Recent studies on a series of [Cp*-Ir^{III}(chelate)X] complexes such as **1** (Fig. 8) show that, under turnover conditions, the initial complexes act as simple pre-catalysts that quickly release the Cp* ligand and forms bis-μ-oxo diiridium(IV) species (Fig. 8, complex **2**). Therefore, the Cp* ligand acts as a placeholder that stabilize the pre-catalysts, then allowing the fast generation of the active dimeric species under catalytic conditions, which retain intact the rest of organic ligands.[50] Following this, O. Diaz-Morales et al recently reported the use of SERS for analyzing the stability and fate of the Cp*-Ir^{III} WOC **3** (Fig. 8) on a polycrystalline gold electrode.[14]

The set of SER spectra shown in Fig. 9 and their comparison with the normal mode Raman spectra of complex **2** and those of the structurally related complexes **4** and **5** (Fig. 8) let the authors reach the following conclusions about the stability and evolution of **1** under electrooxidative conditions

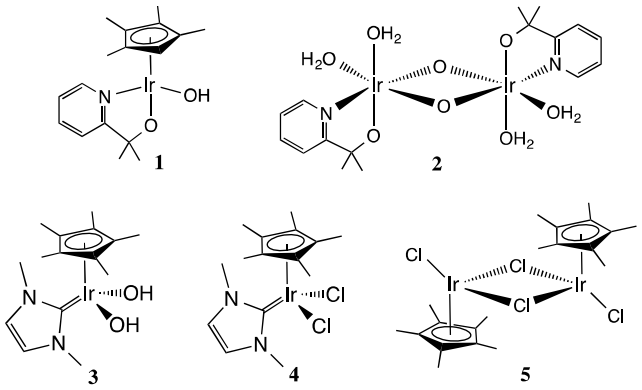

Fig. 8 Drawing of the Cp*-Ir^{III}-N-dimethylimidazolin-2-ylidene WOC **3** studied by SERS and related Cp*-Ir^{III} complexes discussed in this section.

prior to water oxidation: (a) the NHC ligand remains stable though potential cycling as confirmed by the persistence of the C-N stretching peak of the imidazoline moiety at 1031 cm^{-1}, (b) as the persistence a Cp*-Ir stretching peak at about 450 cm^{-1} indicates, the Cp* ligand is not irreversibly lost during oxidative activation (thing that happens for related Cp*-Ir^{III}

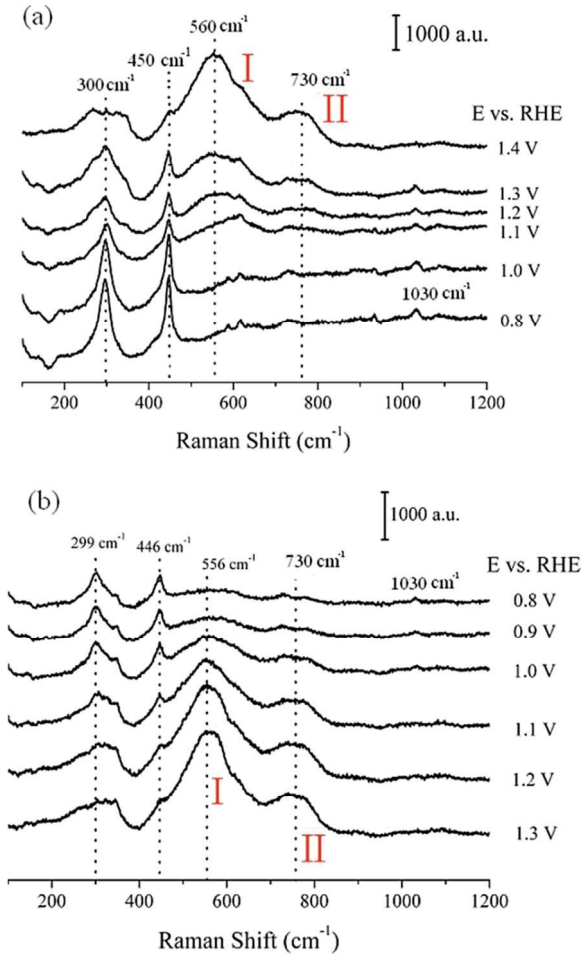

Fig. 9 SERS spectra for WOC **3** on gold (0.1 M $HClO_4$) in the 0.8-1.4 V vs RHE potential range: (a) increasing the potential stepwise from 0.8 V vs RHE and (b) decreasing the potential stepwise from 1.3 V vs RHE. (with permission from ACS)

complexes such as **1** in Fig. 8 under catalytic conditions), (c) a bis-μ-oxo dimer with a related structure to complex **2** (Fig. 8) is proposed as active species formed at high potentials. Peaks marked as I and II at 564 and 733 cm^{-1} in Fig. 9, that show isotopic shift when the spectra are measured in H_2O^{18}, were assigned to two pairs of Ir-O/O-Ir stretches by analogy to the frequencies and shifts reported by Crabtree and co-workers for complex **2** in solution, and (d) **3** does not decompose to IrO_x nanoparticles during electrooxidation as shown by the distinct nature of the Raman peaks observed for both compounds. Further confirmation of the stability of the organic moieties of complex **3** was then obtained by OLEMS (online electrochemical mass spectrometry) as no CO_2 was evolved under turnover conditions.[14]

4. Molecular and catalytic transitions during water oxidation

For the trinuclear Ru-red, the Raman signatures observed during electrochemical SERS studies in solution at E > 0.70 V show shifts of the Ru–O stretching to ~175 cm^{-1} and of the Raman band at 280 cm^{-1} (observed at 0.64 V) to higher wavenumbers, both indicating a transition from Ru-red to Ru-brown at high electrode potentials (Fig. 7b).[17] Subsequently, the Ru-brown type of species further loses electrons and oxidizes water to dioxygen.[45-47] On the other hand, the molecular Cp*-Ir(III) WOC **3** undergoes a molecular transition to a dimeric bis-μ-oxo structure still containing the Cp* ring (Scheme 1) as evident from characteristic Raman Ir-O stretchings appearing at 564 cm^{-1} and 733 cm^{-1} and the persistence of the Cp*-Ir stretching band at about 450 cm^{-1} while increasing the applied potential. Interestingly, in both cases in situ electrochemical SERS data obtained in solution do not lead to any feature indicating the formation of metal oxide species arising from the depletion of the studied molecular systems, thus disgarding its oxidative conversion into heterogeneous RuO_x or IrO_x type species. Therefore, spectroelectrochemical Raman signatures served here to establish the molecular nature of the Ir and Ru-based molecular WOCs studied at the surface of Au electrodes and to shed some light on the fate of these water oxidation catalysts before or under turnover conditions.[14,17]

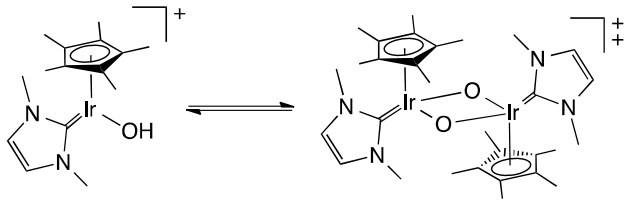

Scheme 1 Molecular transition of the mononuclear Cp*-Ir^{III} WOC **3** to a bis-μ-oxo Ir-dimer.

5. Conclusion and outlook

Surface-enhanced Raman scattering (SERS) is nowadays a well-established vibrational technique that provides high molecular specificity and high sensitivity once the appropriate

setup is disposed; particularly a nanostructured (usually metallic) substrate able to enhance the Raman signal through the excitation of localized surface plasmon resonances (LSPRs) and the formation of charge-transfer species with the analyte, together with the correct placement of the sample in its close proximity. Therefore, among much other applications in diverse fields, this setup is particularly suitable for the study of processes taking place on electroactive surfaces such as, for instance, electrocatalysis.

Both transition-metal based molecular species and inorganic oxides are currently investigated as promising catalysts for the oxidation of water to molecular oxygen, being repeatedly included as part of hybrid anodes intended to electrocatalyse this energy-related transformation. Understanding the evolution of these molecular/oxide species while being oxidized to its active form and under turnover conditions is key for the rational design of improved (both in terms of activity/efficiency and robustness) water oxidation catalysts. Therefore, in this perspective article and by means of few recent studies on the field we highlighted the potential of in situ Raman and SERS techniques for characterizing the fate and unravelling mechanistic details of diverse water oxidation anodes by in situ monitoring their vibrational signatures.

For heterogeneous electrocatalytic materials based on Co, Ni and mixed Ni-Fe oxides in situ Raman spectroscopy at controlled redox potentials allows identifying the different oxide phases formed and the potentials at which they interconvert by analyzing their specific vibrational finguerprint. Correlation of the spectroscopic data with oxygen evolution activity measurements enables extracting key structure-activity relationships such as that disordered NiOOH is the catalytically active species in Ni-Fe mixed oxides or that electropositive metals such as Au in contact with Co oxides triggers the oxidation of the latters to Co(IV) and, consequently, enhance their TOF values by nearly a factor of 40.

For molecular species, the secuential recording of SER spectra at each potential step allows monitoring the molecular changes taking place by the electrochemically driven oxidation of the initial species and inferring about their reversibility while progressively decreasing the applied redox potential. Therefore, as shown for the cases of Ru-red and the Cp*-Ir^{III} WOC **3** commented above, SERs spectroscopy on working water oxidation electrodes is a powerful tecnique that can help on the identification of the real catalytic species or the species entering into the catalytic cycle, on assessing their stability and nature before or under turnover conditions and on confirming or disgarding phase transitions leading to the formation of metal oxides by catalyst depletion under the harsh water oxidation conditions. Considering all this we anticipate that in situ Raman and SERS will become a key tools for the characterization, understanding and rational improvement of water oxidation anodes.

Acknowledgements

K.S.J. acknowledges research funding from the Higher Education Commission (HEC), Government of Pakistan and Leiden University for the research support and facilities. X.S. thanks MINECO CTQ2011-26440 for financial support.

Notes and references

[a] Leiden Institute of Chemistry, Leiden University
Einsteinweg 55, P.O. Box 9502, 2300 RA, Leiden, The Netherlands. E-mail: khurramsj@chem.leidenuniv.nl
[b] Department of Chemistry, University of Engineering and Technology, GT Road, 54890, Lahore, Punjab, Pakistan
[c] Departament de Química, Universitat Autònoma de Barcelona, Cerdanyola del Vallès, 08193 Barcelona, Spain

1 a) K. S. Joya and H. J. M. de Groot, *ChemSusChem,* 2014, **7**, 73; b) K. Ocakoglu, K. S. Joya, E. Harputlu, A. Tarnowska and D. T. Gryko, *Nanoscale*, 2014, **6**, 9625.

2 K. S. Joya, N. K. Subbaiyan, F. D'Souza and H. J. M. de Groot, *Angew. Chem. Int. Ed*., 2012, **51**, 9601.

3 a) M. D. Karkas, O. Verho, E. V. Johnston and B. akermark, *Chem. Rev.*, 2014, **114**, 11863; b) K. S. Joya, J. L. Vallés-Pardo, Y. F. Joya, T. Eisenmayer, B. Thomas, F. Buda and H. J. M. de Groot, *ChemPlusChem*, 2013, **78**, 35.

4 a) K. S. Joya and H. J. M. de Groot, *Int. J. Hydrogen Energy*, 2012, **37**, 8787; b) X. Sala, X., S. Maji, R. Bofill, J. Garcia-Anton, L. Escriche and A. Llobet, *Acc. Chem. Res.*, 2014, **47**, 504.

5 R. D. L. Smith, M. S. Prévot, R. D. Fagan, Z. Zhang, P. A. Sedach, M. K. J. Siu, S. Trudel and C. P. Berlinguette, *Science*, 2013, **340**, 60.

6 L. Trotochaud, J. K. Ranney, K. N. Williams and S. W. Boettcher, *J. Am. Chem. Soc.*, 2012, **134**, 17253

7 J. Suntivich and H. A. Gasteiger, *Nat. Chem*., 2011, **3**, 546.

8 V. Artero and M. Fontecave, *Chem. Soc. Rev.,* 2013, **42**, 2338.

9 D. Hong, J. Jung, J. Park, Y. Yamada, T. Suenobu, Y.-M. Nam and S. Fukuzumi, *Energy Environ. Sci.,* 2012, **5**, 7606.

10 J. J. Stracke and R. G. Finke, *ACS Catal.*, 2014, **4**, 909.

11 D. B. Grotjahn, D. B. Brown, J. K. Martin, D. C. Marelius, M.-C. Abadjian, H. N. Tran, G. Kalyuzhny, K. S. Vecchio, Z. G. Specht, S. A. Cortes-Llamas, V. Miranda-Soto, C. van Niekerk, C. E. Moore and A. L. Rheingold, *J. Am. Chem. Soc.*, 2011, **133**, 19024.

12 K. S. Joya, Y. F. Joya, K. Ocakoglu and R. van de Krol, *Angew. Chem. Int. Ed*., 2013, **52**, 10426.

13 A. Ikeda-Ohno, S. Tsushima, C. Hennig, T. Yaitab and G. Bernhard, *Dalton Trans*., 2012, **41**, 7190.

14 O. Diaz-Morales, T. J. P. Hersbach, D. G. H. Hetterscheid, J. N. H. Reek and M. T. M. Koper, *J. Am. Chem. Soc*., 2014, **136**, 10432.

15 B. S. Yeo and A. T. Bell, *J. Am. Chem. Soc.*, 2011, **133**, 5587.

16 M. W. Louie and A. T. Bell, *J. Am. Chem. Soc.*, 2013, **135**, 12329.

17 K. S. Joya and H. J. M. de Groot, *J. Raman Spec*., 2013, **44**, 1195.

18 S. Schlücker, *Angew. Chem. Int. Ed*., 2014, **53**, 4756 and references there in.

19 B. Sharma, R. R. Frontiera, A.-I. Henry, E. Ringe and R. P. Van Duyne, *Mater. Today*, 2012, **15**, 16.

20 D. J. Gardiner and P. R. Graves (Eds.) Practical Raman spectroscopy, Springer-Verlag, 1989, ISBN 978-0-387-50254-0.

21 L. A. Lyon, C. D. Keating, A. P. Fox, B. E. Baker, L. He, S. R. Nicewarner, S. P. Mulvaney and M. J. Natan, *Anal. Chem*., 1998, **70**, 341.

22 X. Xu, H. Li, D. Hasan, R. S. Ruoff, A. X. Wang and D. L. Fan, *Adv. Funct. Mater.,* 2013, **23**, 4332.

23 M. Fleischmann, P. J. Hendra and A. J. McQuillan, *Chem. Phys. Lett*., 1974, **26**, 163.

24 E. J. Blackie, E. C. Le Ru and P. G. Etchegoin, *J. Am. Chem. Soc*., 2009, **131**, 14466.

25 P. L. Stiles, J. A. Dieringer, N. C. Shah and R. P. Van Duyne, *Annu. Rev. Anal. Chem.*, 2008, **1**, 601.

26 P. Gao, D. Gosztola, L. W. H. Leung and M. J. J. Weaver, *Electroanal. Chem*., 1987, **233**, 211.

27 A. D. McFarland, M. A. Young, J. A. Dieringer and R. P. Van Duyne, *J. Phys. Chem. B*, 2005, **109**, 11279.

28 J. Gan, X. Lu and Y. Tong, *Nanoscale*, 2014, **6**, 7142.

29 N. Morlanés, K.S. Joya, K. Takanabe and V. Rodionov, *Eur. J. Inorg. Chem.*, 2014, DOI:10.1002/ejic.201403015.

30 a) K. S. Joya, K. Takanabe and H. J. M. de Groot *Adv. Energy Mater*., 2014, **4**, DOI: 10.1002/aenm.201400252; b) M. S. Faber and S. Jin, *Energy Environ. Sci.,* 2014, **7**, 3519

31 B. S. Yeo, S. L. Klaus, P. N. Ross, R. A. Mathies and A. T. Bell, *ChemPhysChem*, 2010, **11**, 1854.

32 M. E. G. Lyons and M. P. Brandon, *Int. J. Electrochem. Sci.*, 2008, **3**, 1425.

33 M. E. G. Lyons and M. P. Brandon, *J. Electroanal. Chem.*, 2010, **641**, 119.

34 J. Yang, H. W. Liu, W. N. Martens and R. L. Frost, *J. Phys. Chem. C*, 2010, **114**, 111.T

35 T.. Pauporte, L. Mendoza, M. Cassir, M. C. Bernard and J. Chivot, *J. Electrochem. Soc.*, 2005, **152**, C49.

36 B. E. Conway and T. C. Liu, *Mater. Chem. Phys.*, 1989, **22**, 163–182.

37 a) G. W. Simmons, E. Kellerman and H. Leidheiser, *J. Electrochem. Soc.*, 1976, **123**, 1276; b) G. W. Simmons, A. Vertes, M. L. Varsanyi and H. Leidheiser, H. *J. Electrochem. Soc*., 1979, **126**, 187.

38 C. L. Haynes, A. D. McFarland and R. P. Van Duyne, *Anal. Chem.*, 2005, **77**, 338A.

39 K. S. Joya, Y. F. Joya and H. J. M. de Groot, *Adv. Energy Mater.,* 2014, **4**, DOI: 10.1002/aenm.201301929.

40 D. A. Corrigan, *J. Electrochem. Soc.*, 1987, **134**, 377.

41 B. C. Cornilsen, X. Y. Shan and P. L. Loyselle, *J. Power Sources*, 1990, **29**, 453.

42 S. I. C. de Torresi, K. Provazi, M. Malta and R. M. Torresi, *J. Electrochem. Soc.*, 2001, **148**, A1179; b) M. Vidotti, R. P. Salvador and S. I. C. de Torresi, *Ultrason. Sonochem.*, 2009, **16**, 35; c) M. Vidotti, R. P. Salvador, E. A. Ponzio and S. I. C. de Torresi, *J. Nanosci. Nanotechnol.*, 2007, **7**, 3221.

43 R. Kostecki and F. McLarnon, In Proceedings of the Symposium on Electrode Materials and Processes for Energy Conversion and Storage IV; McBreen, J., Mukerjee, S., Srinivasan, S., Eds.; Electrochemical Society, Inc.: Pennington, NJ, 1997; p viii.

44 a) P. R. Graves, C. Johnston and J. J. Campaniello, *Mater. Res. Bull.*, 1988, **23**, 1651; b) J. Jacob and M. A. Khadar, *J. Appl. Phys.*, 2010, **107**, 114310.

45 M. Yagi, E. Takano and M. Kaneko, *Electrochim. Acta*, 1999, **44**, 2493.

46 M. Itabashi, K. Shoji and K. Itoh, *Chem. Lett.*, 1981, **10**, 491.

47 a) M. Yagi, I. Ogino, A. Miura, Y. Kurimura and M. Kaneko, *Chem. Lett.*, 1995, **24**, 863; b) I. Ogino, K. Nagoshi, M. Yogi and M. Kaneko, *J. Chem. Soc. Faraday Trans.*, 1996, **92**, 3431.

48 J. F. Hull, D. Balcells, J. D. Blakemore, C. D. Incavito, O. Eisenstein, G. W. Brudbig and R. H. Crabtree, *J. Am. Chem. Soc*., 2009, **131**. 8730.

49 A. Savini, P. Belanzoni, G. Bellachioma, C. Zuccacia, D. Zucaccia and A. Macchioni, *Green Chem*., 2011, **13**, 3360.

50 U. Hintermair, W. W. Sheehan, A. R. Parent, D. H. Ess, D. T. Richens, P. H. Vaccaro, G. W. Brudvig and R. H. Crabtree, *J. Am. Chem. Soc.*, 2013, **135**, 10837.

